SECURITY INFORMATION

2419

[redacted]

Copy 275
RM E52B18

[redacted]

NACA RM E52B18

TECH LIBRARY KAFB, NM
0143226

NACA

RESEARCH MEMORANDUM

6725

INVESTIGATION OF A 10-STAGE SUBSONIC AXIAL-FLOW RESEARCH COMPRESSOR

I - AERODYNAMIC DESIGN

By Irving A. Johnsen

Lewis Flight Propulsion Laboratory
Cleveland, Ohio

Classification cancelled (or changed to UNCLASSIFIED)
By Authority of NASA Tech Pub Announcement #122
(OFFICER AUTHORIZED TO CHANGE)
By ..... 28 Jul 58
NAME AND
GRADE OF OFFICER MAKING CHANGE)
24 Mar 61
DATE

[redacted]

NATIONAL ADVISORY COMMITTEE
FOR AERONAUTICS
WASHINGTON
April 28, 1952

319.98/39

[redacted]

PERMANENT

NATIONAL ADVISORY COMMITTEE FOR AERONAUTICS

RESEARCH MEMORANDUM

INVESTIGATION OF A 10-STAGE SUBSONIC AXIAL-FLOW RESEARCH COMPRESSOR

I - AERODYNAMIC DESIGN

By Irving A. Johnsen

2494

SUMMARY

A 10-stage axial-flow compressor was designed for use as a research unit in which the problems associated with the compounding of high performance stages could be studied. The design was based on a symmetrical velocity diagram with constant total enthalpy at all radii. Selected design limitations included a Mach number limit of 0.7, a loading limit ($C_L\sigma$ where C_L is the lift coefficient and σ is the blade-element solidity) which increased progressively from 0.8 to 1.0 through the compressor, a solidity limit of 1.1, an inlet hub-tip ratio of 0.55, and a tip diameter of 20 inches. The application of these design limits with an assumed stage polytropic efficiency of 0.90 gave the following design values: a total-pressure ratio of 6.45 and a weight flow of 57.5 pounds per second at the design tip speed of 869 feet per second.

The over-all performance characteristics of this compressor, as determined experimentally, are included.

INTRODUCTION

The desirability of compactness in axial-flow compressors for gas-turbine power plants requires that multistage units produce high pressure ratios per stage and high mass flows per unit frontal area, while at the same time maintaining high efficiencies. Two-dimensional high-speed cascade results (reference 1) indicated that stage pressure ratios could be realized which were considerably in excess of those currently being obtained in multistage machines. In order to study the possibility of utilizing these high loadings and high relative Mach numbers, a rotor-blade row was designed and investigated (reference 2). The results of this investigation verified the fact that increased pressure ratios were attainable in a single stage without significant penalties in efficiency.

Even with the realization of increased pressure ratio in a single stage, however, it was questionable whether the results were applicable to multistage units. Additional factors which are introduced by multistaging, such as boundary-layer growth, oscillatory radial motion of the

gas through many stages, blade-row matching, off-design operating problems, and the like, may prevent high-stage performance from being realized. Therefore, a multistage axial-flow compressor was designed and constructed in which the attempt was made to achieve higher stage pressure ratios than those in current use, while at the same time maintaining high mass flow and efficiency. This design was intended to provide a research unit in which the problems arising from the compounding of high performance stages could be studied. Inasmuch as it was not feasible to attempt to attain an absolute maximum of performance in each stage of this initial design, design limitations were chosen such that there was reasonable assurance that the desired high-performance multistage research compressor would be obtained. 2494

The compressor design, including the determination of the velocity diagram and the selection of the compressor blading, was conducted in 1947 at the NACA Lewis laboratory based on the best information available at that time. This report summarizes the design procedure and the design characteristics of this 10-stage compressor unit. The overall performance map of the compressor for the operating range from 30 percent to 110 percent of equivalent design speed is included.

SYMBOLS

The following symbols are used in this report:

A	area (sq ft)
a	local velocity of sound (ft/sec)
b	intercept in equation $\Delta\beta = m\alpha + b$
C_L	lift coefficient
$C_{L,i}$	design camber (theoretical C_L for isolated airfoil)
$C_{L\sigma}$	loading limit
g	acceleration of gravity (ft/sec^2)
h	dimensionless ratio of axial component of air velocity to rotor-tip speed
$\bar{h}$	average dimensionless axial velocity across passage
hp	horsepower
K	constant

TECH LIBRARY KAFB, NM
0143226

2494

$\overline{M}$ average axial Mach number across passage

m slope in equation $\Delta\beta = m\alpha + b$

n polytropic exponent

P total or stagnation pressure (lb/sq ft)

p static or stream pressure (lb/sq ft)

Q volume rate of flow (cu ft/sec)

q velocity head, $\frac{V^2}{2g}$, (ft)

R gas constant

r radius (ft)

T total or stagnation temperature (°R)

t static or stream temperature (°R)

U velocity of rotor blade element at radius r (ft/sec)

V absolute air velocity (ft/sec)

W air velocity relative to rotor (ft/sec)

W_f air weight flow (lb/sec)

X ratio of circumferential component of absolute velocity of entering air to rotor-tip speed

Y ratio of change in circumferential component of velocity to rotor-tip speed

Z ratio of blade-element velocity to rotor-tip speed (compressor radius ratio)

α angle of attack (deg)

β absolute inlet-air angle, measured with respect to axis (deg) (fig. 3)

β' inlet-air angle relative to rotor, measured with respect to axis (deg) (fig. 3)

γ	ratio of specific heats, c_p/c_v
$\Delta\beta$	turning angle (deg)
η	adiabatic efficiency
η_p	polytropic efficiency
ρ	static or stream density (lb/cu ft)
ρ_t	total or stagnation density (lb/cu ft)
σ	blade-element solidity, chord/spacing

2494

Subscripts:

e	effective value in velocity diagram corrected to constant axial velocity
h	hub
m	mean
t	tip
θ	circumferential direction
0	station ahead of inlet-guide vanes
1,3,5 . . . 19	station ahead of rotors of 1st, 2nd . . . 10th stages
2,4,6 . . . 20	station ahead of stators of 1st, 2nd . . . 10th stages
21	station ahead of exit vanes
22	station after exit vanes

GENERAL CHARACTERISTICS AND LIMITATIONS

Compressor size. - The attainment of a compressor of minimum size for a given pressure ratio and weight flow requires the consideration of velocity distribution as well as limitations on the turning of the air and the blade relative Mach number. The weight flow desired for this compressor was of the order of 50 pounds per second. On the basis of preliminary design estimates and with the use of the established aerodynamic limitations, the inlet diameter was fixed at 20 inches. This

preliminary estimate also established the fact that the desired pressure ratio of 6 could be obtained in 10 stages.

Compressor configuration. - In a multistage axial-flow compressor, configurations are possible in which the tip diameter, the hub diameter, or both vary from stage to stage through the compressor. As pointed out in reference 3, a progressive increase in tip diameter is desirable for obtaining maximum pressure ratio per stage. However, this advantage is balanced by the fact that (for a given inlet stage), an increase in tip diameter results in very short blades, high ratios of hub-to-tip diameter, and small aspect ratios for a given blade chord. Consequently, tip clearance and annulus losses would be larger than for a comparable constant tip-diameter design. Since construction would also be simplified, a constant tip diameter was selected.

2494

In order to maintain the limiting relative Mach number on each blade row (and thereby obtain a maximum pressure ratio), the hub diameter was progressively increased through the compressor. This served to increase the blade-element velocity at the hub, as well as the axial velocity of the stream, and therefore to maintain the limiting relative Mach number despite the increasing speed of sound through the unit.

Velocity diagram. - The type of velocity diagram used in axial-flow compressor design is vitally important in that it establishes the blade element and stage performance. On the basis of a blade-element analysis, the optimum velocity diagram was found to be symmetrical (reference 3).

In applying the blade-element theory to stage design, it was considered desirable to maintain a constant total enthalpy from hub to tip in order to avoid an energy unbalance that might result in excessive mixing losses. It is shown in reference 3 that the use of a symmetrical velocity diagram with constant total enthalpy gives higher pressure ratio and specific mass flow than the more conventional free-vortex design. This high performance results from the fact that the inlet Mach number is maintained near the imposed limit for all blade elements in both rotor and stator.

In view of the generally desirable pressure ratio and mass-flow characteristics, the symmetrical velocity diagram with constant total enthalpy at all radii was selected for this design.

Stage limitations. - The stage performance of axial-flow compressors is dependent on the limitations imposed on the relative Mach number of the air and the turning done by the blade rows. The Mach number limitation was applied by using a value of 0.7 for flow relative to the compressor rotor (the maximum value exists at the hub in this design). In the calculation used, this results in a Mach number at the following stator hub that is slightly higher than 0.7. This Mach number level was chosen on the basis of performance results obtained with the NACA 8-stage compressor (reference 4). Subsequent data (reference 2) have shown that higher Mach numbers could have been used without serious losses in efficiency; however, the selected Mach number level provides a reasonably high pressure rise and insures high efficiency.

2494

The solidity at the hub for all blade rows was selected as 1.1. This value is of the order of that successfully used in the design reported in reference 4.

There was little information available on the amount of turning that could be imparted to the air under various operating conditions. Therefore, a limitation on $C_L\sigma$ (as was used in reference 4) was adopted because of convenience in calculations. In this particular design, this limitation occurs at the hub and is essentially the same in rotor and stator. The values of $C_L\sigma$ were selected to increase progressively through the compressor ($C_L\sigma$ of 0.8 for the first three stages, 0.9 for the next three stages, and 1.0 for the last four stages).

This variation in the loading limitation through the compressor was selected to improve the off-design operation of the compressor, particularly at speeds lower than design and at low flow. Under these operating conditions, the angle of attack in the first stages is increased. Since lightly loaded blades can be expected to have a wide operating range, the use of a low design value of $C_L\sigma$ results in blades that will accept this increased angle of attack without flow breakdown. In addition, the change in density through the compressor at low speed is proportionally less than the design decrease in area; this successively decreases the angle of attack and therefore unloads the latter stages. These two effects result in more nearly uniform loading through this compressor at low speeds. A more recent and complete analysis of the off-design operating problem in multistage axial-flow compressors has indicated that the optimum loading variation is probably one in which the loading increases in the middle stages and decreases again in the latter stages. However, this selected increase in $C_L\sigma$ through the compressor was expected to provide some improvement in the characteristic under low-speed and low-flow operation.

Mass flow and pressure ratio for first stage. - For gas-turbine power-plant application, a small hub diameter and high axial air velocity are desirable to obtain as high a mass flow as possible consistent

with high pressure ratio. For convenience in establishing the design conditions for the inlet stage, the optimum combination of weight flow and pressure ratio was considered on the basis of useful power input to the air. In order to establish these conditions, the following power parameter (appendix A) was used:

2494

$$K(hp) = \frac{Q}{\pi r_t^2 a_1}\left[\left(\frac{p_3}{p_1}\right)^{\frac{\gamma-1}{\gamma}} - 1.0\right]$$

For given inlet conditions and compressor diameter, and for given limitations of Mach number, lift coefficient, and solidity, this power parameter is a function of the hub-tip ratio z_h and the dimensionless axial velocity of the air at the hub h_h.

In figure 1(a), the power parameter (determined on the basis of the limitations chosen to apply to the first stage) is shown as a function of z_h for various values of h_h. It can be seen that the maximum power is obtained at a hub-tip ratio of the order of 0.55 and that the curves are essentially flat from 0.50 to 0.55. The hub-tip ratio for the inlet stage of the compressor was selected as 0.55.

As shown in figure 1(b), maximum power for the hub-tip ratio of 0.55 is obtained at a dimensionless axial velocity h_h of approximately 0.70. A further consideration that must enter into the choice of h_h at the inlet, however, is the axial-velocity distribution over the rest of the stage. A disadvantage of this symmetrical diagram, constant total-enthalpy design, is the fact that the axial velocity at the rotor tip, particularly at the exit, may become dangerously low. The axial velocity of the air discharged at the rotor tip $h_{2,t}$ was therefore investigated by use of the simplified radial equilibrium approximation, which considers only the balance of centrifugal and pressure forces and neglects the effect of curvature of the streamlines. In order to keep the axial velocity at the rotor tip at a reasonable level, a value of h_h of 0.75 was selected for this design. This provides a higher mass flow and a power input only slightly less than the maximum attainable.

Efficiency. - As pointed out in reference 3, the exact analysis of efficiency of an axial-flow compressor is extremely complex and must be based upon a detailed knowledge of the flow processes involved. However, an indication of the efficiency of the main portion of the flow can be obtained by a consideration of blade-element efficiency. An examination of the velocity diagrams on the basis of blade-profile

losses (fig. 17 of reference 4) showed that the blades of this selected entrance stage operate in the region of peak efficiency with the lowest blade-element efficiency existing at the hub.

A preliminary estimate was made to evaluate the efficiency of succeeding stages on a blade-element basis. This study showed that the shift in blade-element efficiency in succeeding stages is in the direction of increased efficiency. It was recognized that viscous effects probably become more severe in later stages and that these real flow effects modify the blade-element trend. However, on the basis of a blade-element consideration of pressure ratio, weight flow, and efficiency, the choice of velocity distribution appeared reasonable.

2494

Axial-velocity distribution. - In this design, which is based on a symmetrical velocity diagram with constant total enthalpy and simplified radial equilibrium, axial velocities are greatest at the hub. This characteristic permits the use of large values of YU_t over the entire blade height without exceeding the $C_L\sigma$ limitation, and allows a Mach number near the limiting value to occur across the entire blade height, both of which contribute to high performance. The disadvantage of this design, however, is that large axial-velocity changes may take place across the blade rows. Across the rotor tip, for example, a deceleration occurs. If this deceleration is sufficiently rapid, flow separation on the blade surface may result.

In order to establish design velocity diagrams, axial-velocity changes must be evaluated. It is shown theoretically in reference 5 that the effect of radial motion of the gas may be important in the determination of this axial-velocity distribution, particularly when the blade aspect ratio is large. However, the exact determination of axial-velocity distribution (considering the complete radial equilibrium equation) requires a long process of step-by-step calculation, which is somewhat impractical in the case of a multistage compressor. Therefore, for this design, the effect of radial motion was neglected and the axial-velocity distribution (at the stations immediately upstream and downstream of blade rows) was determined solely on the basis of simple equilibrium of pressure and centrifugal force.

Subsequent investigation (reference 6) indicates that the analysis based on simple radial equilibrium gives a reasonable approximation to actual conditions across the rotor. Furthermore, analysis has shown that across a complete stage the differences between the complete radial flow solution of reference 5 and the simple radial equilibrium approximation are small. It therefore appears that the use of simple radial equilibrium relations provided a sufficiently accurate determination of the axial-velocity distribution. The simple radial equilibrium relations are developed in appendix B. Charts for determining average dimensionless axial velocities on this basis are presented in figure 2.

Average axial component of velocity. - In high-performance axial-flow compressors, the problem of reducing the velocity to the value that is required for combustion is a difficult one. A possible solution is to reduce the average axial velocity in passing through the compressor; this would reduce the requirements of the diffuser. It would also increase the blade height (particularly in the latter stages), which would be desirable because of reducing tip clearance and annulus losses. However, this method has three disadvantages:

2494

(1) The relative Mach number is reduced, thus reducing the stage pressure ratio and requiring more stages for a given over-all pressure ratio.

(2) The increase in blade height results in a more extreme axial-velocity profile across the passage of the latter stages, which might result in increased mixing losses in the process of being converted to a uniform flow in the diffuser.

(3) The value of $\Delta p/q$ across a given blade row will be increased, which would have an adverse effect with regard to boundary-layer build-up.

In view of these disadvantages, the design was carried out to maintain the relative Mach number in all stages with one limitation. The average axial Mach number was not permitted to exceed 0.6.

DESIGN CALCULATION METHOD

The basic theory used in the velocity diagram determination is essentially a method proposed by J. Austin King, with velocities expressed nondimensionally as ratios of the rotor tip speed. A typical velocity diagram for the case where axial velocity is constant is shown in figure 3(a). In the design calculation, however, the axial velocity varies through the stage because of (1) variation in hub diameter, (2) compressibility, and (3) the change in axial velocity required to satisfy the condition of simplified radial equilibrium between each blade row. A rotor velocity diagram for the case of a varying axial velocity is shown in figure 3(b). This diagram is corrected to constant axial velocity in order to permit use of cascade data; h_e, W_e, β_e', and $\Delta\beta_e$ are "effective" values. This procedure for correcting to an equivalent constant axial-velocity diagram is in accordance with the recommendation of reference 7. Reference 6 and unpublished data obtained at the Langley laboratory indicate that this correction system is adequate for most applications, although it may over correct when axial-velocity changes are large.

Velocity diagram calculations. - The calculation procedure for determining velocity diagrams through the compressor was as follows:

Step 1:

$Z_h = 0.55$ and $h_h = 0.75$ at the inlet of the first stage

2494

Step 2:

$C_L\sigma = 0.8$ for the first stage

Step 3:

$\bar{h}$ was selected from the design chart for the given values of Z_h, h_h, and $C_L\sigma$

Step 4:

$$Y_h = \frac{C_L\sigma}{2}\sqrt{h_h^2 + \frac{Z_h^2}{4}}$$

as derived in reference 4

Step 5:

$$Y_t = Z_h Y_h$$

Step 6:

$$X_h = \frac{Z_h - Y_h}{2}$$

Step 7:

$$X_t = \frac{1 - Y_t}{2}$$

Step 8:

$$\frac{U_t}{a_h} = \frac{\text{Mach number limit}}{\sqrt{h_h^2 + (Z_h - X_h)^2}} = \frac{0.70}{\sqrt{h_h^2 + (Z_h - X_h)^2}}$$

Step 9:

$$\frac{U_t}{a_t} = \frac{U_t}{a_h}\frac{a_h}{a_t}$$

Substituting the relation derived in appendix B for a_h/a_t gives

$$\frac{U_t}{a_t} = \sqrt{\frac{1}{\frac{1}{(U_t/a_h)^2} + \frac{\gamma-1}{2}\left[\frac{1 - Z_h^2}{4}(1 + Y_h^2) - Y_t \log_e \frac{1}{Z_h}\right]}}$$

2494

Step 10:

The polytropic efficiency of this compressor was estimated as 0.90; for convenience in calculations, the polytropic exponent n was used where

$$\frac{n}{n - 1} = \frac{\gamma}{\gamma - 1}\eta_p$$

Step 11:

Bernoulli's equation written in terms of static-pressure ratio is

$$\frac{p_3}{p_1} = \left[1 + (\gamma - 1)\left(\frac{U_t}{a_1}\right)^2\left(\frac{X_1^2 + h_1^2}{2} - \frac{X_3^2 + h_3^2}{2} + YZ\right)\right]^{\frac{n}{n - 1}}$$

An analysis was made on the effect of the velocity components X and h on stage pressure ratio, and it was established that

$$X_1^2 + h_1^2 \approx X_3^2 + h_3^2$$

This was also found true for succeeding stages; therefore, these terms could be deleted with little error. The pressure ratio was therefore determined as

$$\frac{p_3}{p_1} = \left[1.0 + (\gamma - 1)\left(\frac{U_t}{a_1}\right)^2 YZ\right]^{\frac{n}{n - 1}}$$

Step 12:

$$\frac{\rho_3}{\rho_1} = \left[1.0 + (\gamma - 1)\left(\frac{U_t}{a_1}\right)^2 YZ\right]^{\frac{1}{n - 1}}$$

Step 13:

$$\frac{t_3}{t_1} = \left[1.0 + (\gamma - 1)\left(\frac{U_t}{a_1}\right)^2 YZ\right]$$

Step 14:

$$\frac{U_t}{a_3} = \frac{U_t/a_1}{\sqrt{t_3/t_1}}$$

2494

The static-pressure ratio as determined in step 11 (as well as the density and temperature ratios) varied only slightly from hub to tip because of the variation in a_1, which was small. Therefore, for design purposes, including the determination of the power parameter (appendix A), the pressure ratio was taken as that calculated at the tip station.

Step 15:

At this point, a trial-and-error solution was required to select $Z_{3,h}$ in order that both the Mach number limit at the next stage and the continuity equation were satisfied.

$$\overline{h_3} = \overline{h_1}\,\frac{\left(1 - Z_{1,h}^2\right)}{\left(1 - Z_{3,h}^2\right)}\left(\frac{\rho_1}{\rho_3}\right)$$

Step 16:

Then, from the design chart (fig. 2(a)) for the assumed value of $Z_{3,h}$, the value of $h_{3,h}$ was determined.

Step 17:

Steps (1) to (7) were repeated to satisfy the equation under step 8 at station 3.

$$\sqrt{h_{3,h}^2 + \left(Z_{3,h} - X_{3,h}\right)^2}\left(\frac{U_t}{a_{3,h}}\right) = 0.7$$

The calculation procedure then defined the tentative hub diameter, stage by stage, through the compressor. The calculations were carried through until the number of stages was sufficient to produce an overall total-pressure ratio of approximately 6.

With the tentative hub diameters determined, axial chord lengths and gaps were selected and a curve of rotor hub diameters was established. This curve was then faired to eliminate profile discontinuities and to establish the actual diameters, for rotor and stator, through the compressor. The preceding calculations were then repeated for the new values of hub diameter in order to establish the final design values.

This fairing of the hub diameters resulted in a small deviation
2494 from the 0.7 Mach number limit desired for the hub of the rotor. Actual inlet Mach number values at other stations were established from the relation at the rotor inlet

$$\frac{W}{a} = \frac{W}{U_t}\frac{U_t}{a}$$

and, at the stator inlet

$$\frac{V}{a} = \frac{V}{U_t}\frac{U_t}{a}$$

where, for the general case, the equation under step 9 can be written for rotor inlet

$$\left(\frac{U_t}{a}\right)^2 = \frac{1}{\dfrac{1}{\left(\dfrac{U_t}{a_h}\right)^2} + \dfrac{\gamma-1}{2}\left(\dfrac{Z^2 - Z_h{}^2}{4} - \dfrac{Y_t{}^2}{4Z^2} + \dfrac{Y_h{}^2}{4} - Y_t \log_e \dfrac{Z}{Z_h}\right)}$$

and for stator inlet

$$\left(\frac{U_t}{a}\right)^2 = \frac{1}{\dfrac{1}{\left(\dfrac{U_t}{a_h}\right)^2} + \dfrac{\gamma-1}{2}\left(\dfrac{Z^2 - Z_h{}^2}{4} - \dfrac{Y_t{}^2}{4Z^2} + \dfrac{Y_h{}^2}{4} + Y_t \log_e \dfrac{Z}{Z_h}\right)}$$

Also, for the rotor inlet

$$\left(\frac{W}{U_t}\right)^2 = (X + Y)^2 + h^2$$

and for the stator inlet

$$\left(\frac{V}{U_t}\right)^2 = (X + Y)^2 + h^2$$

This distribution of inlet Mach number across the annulus indicated how well any particular blade row was being utilized.

In selecting the hub diameter for a desired flow variation through the compressor, it is desirable to account for the presence of boundary layer. This, however, requires a precise knowledge of the magnitude of the boundary layer and its variation through the compressor. Because of a lack of pertinent data on the subject at the time of the design, no attempt was made to provide a boundary-layer allowance. It was therefore anticipated that the design weight flow might not be obtained. Furthermore, desired angles of attack might not be maintained, particularly in the latter stages where boundary layer (as a percentage of passage height) is a maximum. However, an observed tendency to obtain greater rotor turning (and therefore pressure ratio) than predicted from low-speed cascade data would tend to provide a balancing effect with regard to angles of attack. 2494

Construction of velocity diagrams. - At any given radius, the rotor-inlet velocity vectors could be established from the data of the calculation procedure and the radial equilibrium relations at the rotor inlet station. Rotor exit vectors for this same radius were then established from: (1) values of h_2 (for the new value of Z_h at the rotor exit) determined on the basis of continuity and simple radial equilibrium at this station and (2) values of X and Y determined in the calculation procedure. It was assumed that the mean density rise across the rotor was one half the stage rise. Then, at the rotor exit, for continuity

$$\bar{h}_2 = \bar{h}_1 \frac{\left(1 - Z_{1,h}^2\right)}{\left(1 - Z_{3,h}^2\right)} \frac{2.0}{\left(1 + \frac{\rho_3}{\rho_1}\right)}$$

Through the use of figure 2(b), the value of $h_{2,h}$ and therefore the value of h_2 at any radius could be obtained for this rotor exit station. Actual and effective values of inlet-air angle and turning angle were calculated.

The velocity vectors for the stator were determined by a similar procedure. For the stator, however, there was a discrepancy introduced by the assumption that the velocity diagrams were symmetrical because the required change in diagram from stage to stage was not considered. Therefore, the stator diagram was so modified that the rotation removed at each radius in the stator Y was that required to provide the desired absolute rotational component X for the following rotor. The velocity diagram therefore deviated from symmetry to a limited extent.

2494

Determination of pressure ratio and weight flow. - The total-pressure ratio of the compressor was established by consideration of the anticipated performance of inlet guide vanes and the exit vanes (designed to remove rotation remaining after the tenth stage) in addition to the 10 stages for which static-pressure ratios were calculated.

$$\frac{P_{22}}{P_0} = \frac{P_{22}}{p_{22}} \frac{p_{22}}{p_{21}} \frac{p_{21}}{p_1} \Big/ \frac{P_0}{p_0} \frac{p_0}{p_1}$$

where

$$\frac{P_0}{p_0} = \left[1.0 + \frac{\gamma-1}{2}\left(\frac{U_t}{a_0}\right)^2 h_0^2\right]^{\frac{\gamma}{\gamma-1}}$$

$$\frac{p_0}{p_1} = \left[1.0 + \frac{\gamma-1}{2}\left(\frac{U_t}{a_1}\right)^2 \left(X_1^2 + h_1^2 - h_0^2\right)\right]^{\frac{n}{n-1}}$$

$$\frac{p_{21}}{p_1} = \frac{p_3}{p_1} \frac{p_5}{p_3} \cdot \cdot \cdot \frac{p_{21}}{p_{19}}$$

$$\frac{P_{22}}{p_{22}} = \left[1.0 + \frac{\gamma-1}{2}\left(\frac{U_t}{a_{22}}\right)^2 h_{22}^2\right]^{\frac{\gamma}{\gamma-1}}$$

$$\frac{p_{22}}{p_{21}} = \left[1.0 + \frac{\gamma-1}{2}\left(\frac{U_t}{a_{21}}\right)^2 \left(X_{21}^2 + h_{21}^2 - h_{22}^2\right)\right]^{\frac{n}{n-1}}$$

For the inlet guide vanes, a polytropic expansion efficiency of 0.85 was assumed; for the exit vanes, a polytropic compression efficiency of 0.85 was used. Corresponding density relations were determined using these equations with the required changes in exponents.

Compressor weight flow was established from

$$W_f = \rho_1 \bar{h}_1 U_t A_1$$

where

$$\rho_1 = \frac{\rho_{t,0}}{\left[1 + \frac{\gamma-1}{2}\left(\frac{U_t}{a_0}\right)^2 h_0^2\right]^{\frac{1}{\gamma-1}}\left[1 + \frac{\gamma-1}{2}\left(\frac{U_t}{a_1}\right)^2 (X_1^2 + h_1^2 - h_0^2)\right]^{\frac{1}{n-1}}}$$

2494

Since W_f, h_0, and a_0 were unknown, the solution for pressure ratio and weight flow (assuming standard sea-level values for inlet stagnation conditions) required iteration which started with the assumption that

$$h_0 = h_1$$

and

$$a_0 = a_1$$

This provided a first approximation to ρ_1 and therefore W_f. Then

$$\rho_0 = \frac{\rho_{t,0}}{\left[1.0 + \frac{\gamma-1}{2}\left(\frac{U_t}{a_0}\right)^2 h_0^2\right]^{\frac{1}{\gamma-1}}}$$

$$h_0 = \frac{W_f}{\rho_0 U_t A_0}$$

and

$$a_0 = \sqrt{\gamma g R T_0 \left(\frac{\rho_0}{\rho_{t,0}}\right)^{\gamma-1}}$$

from which ρ_1 could be determined. A single iteration was found to give sufficiently accurate values of ρ_1 and W_f. With the weight flow established, the conditions at station 22 were determined in similar manner.

AIRFOIL SELECTION

With the values of stagger angle and turning angle established, compressor airfoils were selected for the various stages, including the exit vanes. The design used the NACA 65-series airfoil scaled down to 10 percent thickness and modified by the addition of 0.0015 times chordal position to the thickness ordinate, designated in reference 7 as the NACA 65-series blower blade section.

2494

In order to simplify construction, the blades were designed with constant camber and chord at all radii of a given blade row rather than using a variable section blade. Thus the solidity varies inversely with the radius in any stage.

In selecting blades, data from references 7, 8, and 9 were used. The guide vane data of reference 9 were used because no suitable data were available in the low inlet-air-angle range; interpolation was therefore necessary. The use of this zero inlet-air-angle data as an end point appeared to be reasonably accurate.

The design charts of reference 8 provide a method of selecting optimum camber (represented by the free-stream lift coefficient for zero incidence $C_{L,i}$) and angle of attack α. The data were extended to cover low inlet-air angles and low solidities by a series of cross-plots, using the data of reference 9 as a guide. Reasonable consistency was obtained and the data were put in chart form (fig. 4) so that values of $C_{L,i}$ and α could be selected for given values of β, $\Delta\beta$, and σ.

With the desired solidity at the root and with a selected axial projection of each blade, an approximation to the number of blades in each row was made. The actual number of blades in each row was then determined from a consideration of blade exciting forces; a common denominator was avoided in adjacent rows.

Through the use of figure 4, values of $C_{L,i}$ were determined at five radii in each blade row. It was found that the optimum blade sections for this compressor had minimum camber at the tip and maximum camber at the root. An intermediate value was chosen as the constant-camber section of the blade row, thus obtaining optimum blading near the pitch radius and departing slightly at root and tip. The camber was chosen to maintain the same blade section for both rotor and stator wherever possible.

With the blade section established, it was necessary to establish the angle of attack necessary to obtain the required turning at each radial station. Examination of the data of references 7, 8, and 9

indicated that these turning data could be roughly approximated by a straight line variation of $\Delta\beta$ with respect to α. The equation used was

$$\Delta\beta = m\alpha + b$$

2494

Charts (fig. 5) were prepared for the determination of m (as a function of β and σ) and b (as a function of β, $C_{L,i}$, and σ) from the available data on 65-series blower blade sections. The maximum difference between the cascade test data and the turning angle determined from the charts was of the order of 1°, with the nominal variation of the order of $1/2^{\circ}$. With the use of these charts, the value of α required to accomplish the design turning at each of 5 radial stations was determined.

With the blade angle known and with the projected chord and number of blades specified, the actual chord and the solidity of each blade row could be determined. It was also possible to establish the actual value of C_L from the relation

$$C_L = \frac{2U_tY}{W_m\sigma}$$

Reference 10 (table II) gives the mean line data for the NACA 65-series blower blade sections with $C_{L,i} = 1.0$. For the prescribed camber, the coordinates of the mean line and the tangent of the angle of the mean line were obtained by multiplying by the design value of $C_{L,i}$. By the use of the data given in reference 10 (table I) for a 10 percent thick NACA 65-series blower blade section, the coordinates of the airfoil were determined.

Sheet-metal inlet guide vanes were selected to provide the turning as established by the inlet-stage velocity diagram. Blade sections were chosen by use of the methods subsequently published in references 11 and 12, which considered both two-dimensional blade-element performance and secondary flow effects resulting from the radial distribution of design circulation.

DESIGN CHARACTERISTICS

The various design characteristics determined in the design procedure are as follows (values given are for standard sea-level inlet conditions):

Over-all total-pressure ratio	6.45
Average stage total-pressure ratio	1.205
Weight flow, lb/sec (no boundary layer allowance)	57.5
Weight flow per unit frontal area, lb/sec	26.4
Tip speed, ft/sec	869
Tip speed, rpm	9959
Over-all adiabatic efficiency	0.86

2494

The values of static-pressure ratio per stage are plotted in figure 6(a). The discontinuities in the plot are a result of the change in the $C_L\sigma$ limitation through the compressor. Ratio of static pressure ratio to the total pressure at the compressor inlet is shown in figure 6(b); total-pressure ratio is shown in figure 6(c).

The average dimensionless axial velocity $\bar{h}$ and the average axial Mach number $\bar{M}$ entering each stage of the compressor are shown in figure 7. The distribution of axial velocity across the annulus is shown in figure 8. Figure 8(a) represents the dimensionless axial velocity at the entrance to each rotor; figure 8(b) represents the dimensionless axial velocity at the station corresponding to the stator entrance.

The values of hub radius, blade chord, axial projection of the blade chord at the hub, number of blades, design camber, and maximum thickness of blades are given in table I for both rotor and stator rows. A summary of the velocity diagram data is given in table II for rotor and stator rows; values of Z, X, Y, h, W/U_t, V/U_t, W/a, V/a, β', and β are listed for five equally spaced stations at rotor and stator entrance. Changes through the given blade row (Δh and $\Delta\beta$) and blade data (α, $C_L\sigma$, and σ) are also included.

OVER-ALL TEST RESULTS

The compressor was tested in accordance with the standard procedure of reference 13; characteristics as determined experimentally are presented in figure 9. At design speed the peak compressor pressure ratio was 7.52, the maximum weight flow was 56.2 pounds per second, and the peak adiabatic efficiency was 0.83. The experimentally determined performance is discussed in greater detail in reference 14.

SUMMARY OF DESIGN PROCEDURE

The design of the 10-stage axial-flow compressor was based on the use of a symmetrical velocity diagram with constant total enthalpy at all radii. The configuration chosen had a constant tip diameter of 20 inches, an inlet hub-tip ratio of 0.55, and a hub diameter which increased at the rate required to maintain the selected limiting Mach

number for the blade rows. Aerodynamic limitations used included a relative Mach number limit of 0.7, a solidity of 1.1, and a loading limit ($C_L\sigma$ where C_L is the lift coefficient and σ is the blade-element solidity) which increased from 0.8 to 1.0 through the compressor. The axial velocity entering the compressor was chosen to approach closely maximum useful power input for the inlet stage. Axial-velocity distributions through the compressor were established by the simplified radial equilibrium approximation. Velocity diagrams were determined throughout the compressor, and 65-series blower blades were selected to accomplish the required turning from available cascade data. 2494

This design procedure with an assumed stage polytropic efficiency of 0.90 established the following design-point characteristics: a pressure ratio of 6.45 and an equivalent weight flow of 57.5 pounds per second at the design equivalent tip speed of 869 feet per second.

Lewis Flight Propulsion Laboratory
National Advisory Committee for Aeronautics
Cleveland, Ohio

2494

APPENDIX A

DERIVATION OF POWER PARAMETER

The useful power of the inlet stage of this design can be approximated by the following equation, since the change in velocity across the stage is small:

$$hp = \frac{\frac{\gamma}{\gamma-1} p_1 Q_1 \left[\left(\frac{p_3}{p_1}\right)^{\frac{\gamma-1}{\gamma}} - 1.0\right]}{550}$$

Transposing and dividing by $\pi r_t^2 a_1$ gives

$$\frac{550\ hp}{\frac{\gamma}{\gamma-1} p_1\ \pi r_t^2 a_1} = \frac{Q_1}{\pi r_t^2 a_1}\left[\left(\frac{p_3}{p_1}\right)^{\frac{\gamma-1}{\gamma}} - 1.0\right]$$

For given inlet conditions and compressor diameter,

$$K(hp) = \frac{Q_1}{\pi r_t^2 a_1}\left[\left(\frac{p_3}{p_1}\right)^{\frac{\gamma-1}{\gamma}} - 1.0\right]$$

where

$$\frac{Q_1}{\pi r_t^2 a_1} = (1 - Z_{1,h}^2)\ \bar{h}_1 \left(\frac{U_t}{a_1}\right)$$

(for a given $C_L\sigma$ limit, the average axial velocity $\bar{h}$ is a function of h_h and Z_h) and

$$\frac{p_3}{p_1} = \left[1.0 + (\gamma-1)\left(\frac{U_t}{a_1}\right)^2 YZ\right]^{\frac{n}{n-1}}$$

as developed in step 11.

2494

2494

APPENDIX B

DETERMINATION OF AXIAL VELOCITY

The axial velocity at the various stations and radii through the compressor was determined from consideration of the simplified radial equilibrium relation

$$\frac{dp}{dr} = \frac{\rho V_\theta^{\,2}}{r} = \frac{\rho(XU_t)^2}{r}$$

$$= \frac{K(p)^{\frac{1}{\gamma}}\,(XU_t)^2}{r}$$

For the symmetrical diagram (fig. 3(a)), at the rotor entrance

$$XU_t = \frac{ZU_t}{2} - \frac{YU_t}{2}$$

and since

$$Y = \frac{Y_t}{Z}$$

$$XU_t = \frac{ZU_t}{2} - \frac{Y_tU_t}{2Z}$$

Therefore,

$$\frac{dp}{Kp^{\frac{1}{\gamma}}} = \frac{U_t^{\,2}}{4}\left(Z - \frac{Y_t}{Z}\right)^2 \frac{dr}{r} = \frac{U_t^{\,2}}{4}\left(Z - \frac{Y_t}{Z}\right)^2 \frac{dZ}{Z}$$

Integrating between the hub and a given radius yields

$$\frac{1}{K}\,\frac{\gamma}{\gamma-1}\left(p^{\frac{\gamma-1}{\gamma}} - p_h^{\frac{\gamma-1}{\gamma}}\right) = \frac{U_t^{\,2}}{4}\left[\frac{Z^2 - Z_h^{\,2}}{2} - 2Y_t \log_e \frac{Z}{Z_h} - \frac{1}{2}\,Y_t^{\,2}\left(\frac{1}{Z^2} - \frac{1}{Z_h^{\,2}}\right)\right]$$

But

$$a^2 = \frac{\gamma p}{K}^{\frac{\gamma-1}{\gamma}}$$

Therefore,

$$\frac{a^2}{\gamma-1}\left[1 - \left(\frac{a_h}{a}\right)^2\right] = \frac{U_t^2}{4}\left(\frac{Z^2 - Z_h^2}{2} - 2Y_t \log_e \frac{Z}{Z_h} - \frac{1}{2}\frac{Y_t^2}{Z^2} + \frac{Y_h^2}{2}\right)$$

2494

$$\left(\frac{a_h}{a}\right)^2 = 1 - \left(\frac{\gamma-1}{2}\right)\left(\frac{U_t}{a}\right)^2 \left(\frac{Z^2 - Z_h^2}{4} - Y_t \log_e \frac{Z}{Z_h} - \frac{Y_t^2}{4Z^2} + \frac{Y_h^2}{4}\right)$$

For the assumed condition of constant total enthalpy

$$V_h^2 + 2g\frac{\gamma}{\gamma-1}Rt_h = V^2 + 2g\frac{\gamma}{\gamma-1}Rt$$

$$\frac{U_t^2}{a^2}(h_h^2 + X_h^2) + \frac{2}{\gamma-1}\left(\frac{a_h}{a}\right)^2 = \frac{U_t^2}{a^2}(h^2 + X^2) + \frac{2}{\gamma-1}$$

Substituting the sonic velocity relation gives

$$h^2 + X^2 = h_h^2 + X_h^2 - \left(\frac{Z^2 - Z_h^2}{4} - Y_t \log_e \frac{Z}{Z_h} - \frac{Y_t^2}{4Z^2} + \frac{Y_h^2}{4}\right)$$

With the substitution of $X_h = \frac{Z_h - Y_h}{2}$, $X = \frac{Z - \frac{Y_t}{Z}}{2}$, and $Z_hY_h = Y_t$,

$$h = \sqrt{h_h^2 + \frac{Z_h^2}{2} - \frac{Z^2}{2} + Z_hY_h \log_e \frac{Z}{Z_h}}$$

This equation established the distribution of axial velocity ahead of the rotor in terms of the axial velocity at the hub.

The value of Y_h for a symmetrical velocity diagram was found by the simplified lift consideration outlined in reference 4 as

$$Y_h = \frac{C_L\sigma}{2}\sqrt{h_h^2 + \frac{Z_h^2}{4}}$$

For design purposes, it was also necessary to establish the average dimensionless axial velocity for use in continuity relations. When no variation in density from hub to tip is assumed,

2494

$$\bar{h} = \frac{2}{1 - Z_h^2}\int_{Z_h}^{Z_t} hZ\ dZ$$

$$\bar{h} = \frac{1}{1 - Z_h^2}\int_{Z_h}^{1} Z\sqrt{\left(4h_h^2 + 2Z_h^2 - 2Z^2 + 4Z_hY_h \log_e \frac{Z}{Z_h}\right)}\ dZ$$

In order to expedite design, this equation was integrated graphically and a design chart was prepared where $\bar{h}$ is shown as a function of Z_h, h_h, and $C_L\sigma$ (fig. 2(a)).

For the station at the stator entrance, the value of h was found similarly as

$$h = \sqrt{h_h^2 + \frac{Z_h^2}{2} - \frac{Z^2}{2} - Z_hY_h \log_e \frac{Z}{Z_h}}$$

A chart for the determination of $\bar{h}$ at the stator entrance was prepared for this station (fig. 2(b)).

REFERENCES

1. Bogdonoff, Seymour M.: N.A.C.A. Cascade Data for the Blade Design of High-Performance Axial-Flow Compressors. Jour. Aero. Sci., vol. 15, no. 2, Feb. 1948, pp. 89-95.

2. Dugan, Paul D., Mahoney, John J., and Benser, William A.: Effect of Mach Number on Performance of an Axial-Flow Compressor Rotor-Blade Row. NACA RM E8D29, 1948.

3. Sinnette, John T., Jr.: Analysis of Effect of Basic Design Variables on Subsonic Axial-Flow-Compressor Performance. NACA Rep. 901, 1948. (Formerly NACA RM E7D28.)

4. Sinnette, John T., Jr., Schey, Oscar W., and King, J. Austin: Performance of NACA Eight-Stage Axial-Flow Compressor Designed on the Basis of Airfoil Theory. NACA Rep. 758, 1943. (Formerly NACA ACR E4H18.)

5. Wu, Chung-Hua, and Wolfenstein, Lincoln: Application of Radial-Equilibrium Condition to Axial-Flow Compressor and Turbine Design. NACA Rep. 955, 1950. (Formerly NACA TN 1795.)

6. Burtt, Jack R.: Investigation of Performance of Typical Inlet Stage of Multistage Axial-Flow Compressor. NACA RM E9E13, 1949.

7. Bogdonoff, Seymour M., and Bogdonoff, Harriet E.: Blade Design Data for Axial-Flow Fans and Compressors. NACA ACR L5F07a, 1945.

8. Bogdonoff, Seymour M., and Hess, Eugene E.: Axial-Flow Fan and Compressor Blade Design Data at 52.5° Stagger and Further Verification of Cascade Data by Rotor Tests. NACA TN 1271, 1947.

9. Zimney, Charles M., and Lappi, Viola M.: Data for Design of Entrance Vanes from Two-Dimensional Tests of Airfoils in Cascade. NACA ACR L5G18, 1945.

10. Herrig, L. Joseph, Emery, James C., and Erwin, John R.: Systematic Two-Dimensional Cascade Tests of NACA 65-Series Compressor Blades at Low Speeds. NACA RM L51G31, 1951.

11. Lieblein, Seymour: Turning-Angle Design Rules for Constant-Thickness Circular-Arc Inlet Guide Vanes in Axial Annular Flow. NACA TN 2179, 1950.

12. Lieblein, Seymour, and Ackley, Richard H.: Secondary Flows in Annular Cascades and Effects on Flow in Inlet Guide Vanes. NACA RM E51G27, 1951.

13. NACA Subcommittee on Compressors: Standard Procedures for Rating and Testing Multistage Axial-Flow Compressors. NACA TN 1138, 1946.

14. Budinger, Ray E., and Thomson, Arthur R.: Investigation of a 10-Stage Subsonic Axial-Flow Research Compressor. II - Preliminary Analysis of Over-All Performance. NACA RM E52C04, 1952.

2494

2494

TABLE I - BLADE DATA

Stage	Blade	Hub radius at entrance (in.)	Number of blades	Blade chord (in.)	Axial projection of chord at hub radius	Design camber $C_{L,i}$	Maximum thickness (percent of chord)
1	Rotor	5.500	25	1.550	1.506	0.91	10
1	Stator	5.822	27	1.550	1.501	.91	10
2	Rotor	6.131	28	1.510	1.453	0.93	10
2	Stator	6.420	29	1.510	1.452	.93	10
3	Rotor	6.696	31	1.465	1.397	0.95	10
3	Stator	6.952	33	1.465	1.401	1.025	10
4	Rotor	7.197	34	1.420	1.348	1.110	10
4	Stator	7.424	35	1.420	1.346	1.110	10
5	Rotor	7.639	37	1.380	1.300	1.120	10
5	Stator	7.838	39	1.380	1.298	1.120	10
6	Rotor	8.026	41	1.330	1.247	1.120	10
6	Stator	8.199	43	1.330	1.254	1.200	10
7	Rotor	8.361	45	1.280	1.201	1.280	10
7	Stator	8.508	46	1.280	1.202	1.280	10
8	Rotor	8.647	47	1.225	1.149	1.300	10
8	Stator	8.771	49	1.225	1.150	1.300	10
9	Rotor	8.885	51	1.175	1.101	1.300	10
9	Stator	8.988	53	1.175	1.103	1.300	10
10	Rotor	9.085	56	1.120	1.051	1.300	10
10	Stator	9.174	59	1.120	1.054	1.300	10
	Exit vane	9.262	59	1.120	1.117	0.660	10

TABLE II - VELOCITY DIAGRAM DATA

(a) For rotor rows

Station	Entrance vector data							Change through row		Blade data		
	Z	X	Y	h	$\frac{W}{U_t}$	$\frac{W}{a}$	β'	Δh	Δβ	α	$C_L\sigma$	σ
1	0.5500	0.1153	0.3195	0.7500	0.8669	0.7000	30.10	0.0980	22.36	16.44	0.7562	1.122
	.6625	.1987	.2652	.7259	.8615	.6952	32.58	.0604	18.40	13.46	.6425	.931
	.7750	.2742	.2267	.6883	.8513	.6862	36.04	.0257	15.03	11.24	.5659	.796
	.8875	.3448	.1980	.6357	.8359	.6726	40.49	-.0092	11.66	9.20	.5132	.697
	1.0000	.4122	.1757	.5646	.8151	.6545	46.20	-.0494	7.54	6.80	.4774	.617
3	0.6131	0.1449	0.3233	0.7479	0.8824	0.6969	32.05	0.0925	22.27	16.34	0.7595	1.098
	.7098	.2153	.2792	.7242	.8769	.6922	34.33	.0589	18.96	13.86	.6703	.948
	.8065	.2804	.2458	.6902	.8679	.6843	37.32	.0272	15.97	11.76	.6061	.835
	.9032	.3419	.2194	.6451	.8552	.6735	41.03	-.0052	12.91	9.91	.5588	.746
	1.0000	.4009	.1982	.5868	.8386	.6592	45.59	-.0415	9.27	7.79	.5248	.673
5	0.6696	0.1700	0.3297	0.7533	0.9040	0.6971	33.56	0.0829	22.07	16.05	0.7645	1.079
	.7522	.2294	.2935	.7311	.8988	.6926	35.57	.0530	19.26	14.02	.6939	.961
	.8348	.2852	.2645	.7014	.8912	.6863	38.09	.0241	16.63	12.28	.6400	.866
	.9174	.3384	.2407	.6636	.8808	.6775	41.11	-.0055	13.90	10.60	.5983	.788
	1.0000	.3896	.2208	.6167	.8677	.6666	44.71	-.0381	10.76	8.85	.5667	.723
7	0.7197	0.1709	0.3779	0.7591	0.9367	0.7042	35.87	0.0770	24.32	17.51	0.8637	1.067
	.7898	.2227	.3444	.7407	.9328	.7010	37.44	.0473	21.66	15.59	.8006	.972
	.8599	.2718	.3163	.7169	.9273	.6965	39.36	.0179	19.06	14.00	.7498	.894
	.9300	.3188	.2925	.6873	.9198	.6903	41.65	-.0122	16.37	12.31	.7093	.826
	1.0000	.3640	.2720	.6517	.9106	.6827	44.30	-.0446	13.35	10.59	.6768	.768
9	0.7639	0.1899	0.3842	0.7636	0.9554	0.6973	36.94	0.0715	24.13	17.33	0.8673	1.064
	.8230	.2332	.3566	.7471	.9518	.6943	38.29	.0457	21.90	15.69	.8169	.988
	.8820	.2746	.3328	.7267	.9471	.6906	39.89	.0203	19.71	14.28	.7750	.922
	.9410	.3146	.3119	.7024	.9412	.6859	41.73	-.0058	17.43	12.91	.7399	.864
	1.0000	.3533	.2935	.6737	.9340	.6801	43.83	-.0333	14.94	11.49	.7109	.813
11	0.8026	0.2045	0.3937	0.7775	0.9810	0.6946	37.57	0.0645	23.92	17.08	0.8711	1.081
	.8520	.2406	.3709	.7632	.9780	.6923	38.70	.0425	22.07	15.73	.8309	1.019
	.9013	.2754	.3506	.7464	.9742	.6893	39.99	.0205	20.24	14.58	.7961	.963
	.9507	.3092	.3324	.7268	.9695	.6857	41.44	-.0018	18.34	13.44	.7662	.914
	1.0000	.3420	.3160	.7043	.9639	.6815	43.05	-.0250	16.33	12.32	.7405	.868
13	0.8361	0.1935	0.4492	0.7952	1.0224	0.7021	38.97	0.0592	26.21	18.69	0.9716	1.094
	.8771	.2245	.4282	.7843	1.0203	.7005	39.77	.0384	24.51	17.45	.9354	1.045
	.9181	.2545	.4091	.7716	1.0177	.6985	40.70	.0176	22.83	16.38	.9037	.999
	.9591	.2838	.3916	.7572	1.0147	.6963	41.73	-.0035	21.10	15.30	.8752	.956
	1.0000	.3122	.3756	.7409	1.0110	.6935	42.87	-.0252	19.30	14.29	.8504	.917
15	0.8647	0.2022	0.4604	0.8129	1.0487	0.6960	39.18	0.0550	26.07	18.87	0.9743	1.060
	.8986	.2278	.4430	.8039	1.0470	.6948	39.84	.0376	24.69	17.88	.9453	1.020
	.9324	.2527	.4270	.7937	1.0450	.6934	40.58	.0202	23.33	17.06	.9192	.983
	.9662	.2771	.4120	.7824	1.0426	.6916	41.37	.0025	21.92	16.21	.8951	.949
	1.0000	.3010	.3981	.7698	1.0399	.6897	42.24	-.0153	20.49	15.30	.8734	.916
17	0.8885	0.2074	0.4737	0.8366	1.0788	0.6922	39.15	0.0504	25.99	18.72	0.9772	1.074
	.9164	.2286	.4593	.8293	1.0775	.6913	39.68	.0358	24.88	17.92	.9537	1.041
	.9443	.2493	.4457	.8212	1.0758	.6901	40.24	.0213	23.76	17.18	.9319	1.010
	.9722	.2697	.4329	.8123	1.0740	.6888	40.86	.0067	22.63	16.45	.9118	.982
	1.0000	.2896	.4209	.8027	1.0720	.6874	41.51	-.0080	21.49	15.85	.8933	.954
19	0.9085	0.2087	0.4912	0.8710	1.1174	0.6933	38.78	0.0498	26.01	18.49	0.9780	1.099
	.9314	.2261	.4792	.8652	1.1162	.6925	39.19	.0379	25.13	17.95	.9590	1.072
	.9543	.2433	.4677	.8590	1.1151	.6918	39.61	.0260	24.24	17.30	.9410	1.047
	.9772	.2603	.4567	.8522	1.1137	.6908	40.08	.0141	23.36	16.67	.9239	1.022
	1.0000	.2769	.4463	.8450	1.1122	.6898	40.56	.0022	22.46	16.10	.9081	.998

2494

TABLE II - VELOCITY DIAGRAM DATA - Concluded

(b) For stator rows

Station	Entrance vector data							Change through row		Blade data		
	Z	X	Y	h	$\frac{V}{U_t}$	$\frac{V}{a}$	β	Δh	Δβ	α	$C_L\sigma$	σ
2	0.5822	0.1209	0.3211	0.8312	0.9414	0.7578	28.00	-0.0779	18.88	13.74	0.7639	1.143
	.6866	.1990	.2722	.7718	.9043	.7247	31.40	-.0410	16.17	11.91	.6617	.970
	.7911	.2703	.2363	.7026	.8661	.6912	35.79	-.0063	14.57	10.87	.5906	.842
	.8955	.3371	.2087	.6194	.8256	.6559	41.39	.0298	13.95	10.37	.5401	.744
	1.0000	.4009	.1869	.5152	.7816	.6183	48.77	.0716	14.43	10.41	.5049	.666
4	0.6420	0.1491	0.3262	0.8240	0.9513	0.7476	29.98	-0.0649	18.87	14.04	0.7667	1.086
	.7315	.2149	.2863	.7692	.9181	.7189	33.09	-.0318	16.84	12.67	.6865	.952
	.8210	.2761	.2551	.7067	.8841	.6895	36.93	.0002	15.59	11.76	.6268	.849
	.9105	.3340	.2301	.6335	.8482	.6591	41.68	.0337	15.09	11.36	.5822	.766
	1.0000	.3896	.2095	.5453	.8101	.6271	47.69	.0714	15.41	11.31	.5492	.697
6	0.6952	0.1520	0.3544	0.8206	0.9643	0.7385	31.68	-0.0563	20.43	14.62	0.8259	1.107
	.7714	.2094	.3194	.7711	.9350	.7138	34.44	-.0250	18.76	13.45	.7571	.998
	.8476	.2634	.2906	.7156	.9050	.6798	37.75	.0059	17.69	12.84	.7030	.908
	.9238	.3147	.2667	.6524	.8738	.6631	41.71	.0378	17.20	12.55	.6609	.833
	1.0000	.3640	.2464	.5786	.8411	.6365	46.53	.0731	17.35	12.12	.6279	.770
8	0.7424	0.1736	0.3808	0.8210	0.9907	0.7376	34.03	-0.0523	21.31	15.46	0.8712	1.066
	.8068	.2215	.3504	.7756	.9636	.7153	36.41	-.0236	20.00	14.61	.8142	.980
	.8712	.2672	.3245	.7257	.9363	.6839	39.19	.0051	19.11	14.14	.7676	.908
	.9356	.3110	.3021	.6701	.9082	.6704	42.45	.0347	18.64	13.76	.7294	.846
	1.0000	.3533	.2827	.6071	.8793	.6472	46.33	.0667	18.66	13.65	.6986	.791
10	0.7838	0.1903	0.3888	0.8212	1.0050	0.7257	35.19	-0.0390	21.52	15.37	0.8744	1.093
	.8379	.2304	.3637	.7817	.9818	.7072	37.23	-.0141	20.52	14.61	.8289	1.022
	.8919	.2688	.3417	.7389	.9585	.6889	39.56	.0110	19.84	14.22	.7904	.960
	.9460	.3060	.3221	.6920	.9346	.6701	42.23	.0368	19.45	13.96	.7577	.906
	1.0000	.3420	.3047	.6404	.9101	.6510	45.28	.0639	19.38	13.85	.7302	.857
12	0.8199	0.1809	0.4217	0.8296	1.0253	0.7177	35.99	-0.0306	23.23	16.56	0.9334	1.110
	.8650	.2154	.3997	.7958	1.0058	.6907	37.70	-.0080	22.41	15.97	.8941	1.052
	.9100	.2487	.3799	.7598	.9861	.6875	39.60	.0145	21.79	15.51	.8599	1.001
	.9550	.2809	.3621	.7212	.9662	.6724	41.72	.0376	21.41	15.36	.8301	.954
	1.0000	.3122	.3458	.6793	.9458	.6570	44.09	.0617	21.24	15.18	.8041	.910
14	0.8508	0.1915	0.4546	0.8432	1.0623	0.7195	37.46	-0.0269	24.26	17.28	0.9782	1.102
	.8881	.2199	.4356	.8139	1.0450	.7066	38.85	-.0071	23.60	16.97	.9459	1.055
	.9254	.2476	.4180	.7830	1.0277	.6937	40.37	.0129	23.09	16.58	.9167	1.013
	.9627	.2746	.4018	.7504	1.0102	.6808	42.03	.0332	22.72	16.32	.8904	.974
	1.0000	.3010	.3868	.7157	.9926	.6679	43.86	.0541	22.50	16.24	.8670	.937
16	0.8771	0.1986	0.4669	0.8583	1.0861	0.7107	37.79	-0.0190	24.48	17.57	0.9804	1.090
	.9079	.2222	.4510	.8340	1.0718	.7005	38.91	-.0024	23.95	17.21	.9540	1.052
	.9386	.2451	.4362	.8086	1.0574	.6903	40.12	.0143	23.53	16.88	.9299	1.018
	.9693	..2676	.4224	.7822	1.0430	.6799	41.42	.0311	23.21	16.75	.9080	.986
	1.0000	.2896	.4094	.7545	1.0285	.6697	42.81	.0482	22.97	16.64	.8878	.955
18	0.8988	0.2011	0.4824	0.8790	1.1135	0.7044	37.87	-0.0057	24.90	17.72	0.9830	1.103
	.9241	.2206	.4692	.8590	1.1016	.6964	38.77	.0081	24.50	17.51	.9617	1.073
	.9494	.2397	.4566	.8383	1.0897	.6879	39.71	.0220	24.14	17.26	.9417	1.045
	.9747	.2584	.4448	.8169	1.0779	.6797	40.72	.0362	23.87	17.09	.9233	1.017
	1.0000	.2769	.4335	.7947	1.0660	.6715	41.79	.0503	23.65	16.98	.9060	.991
20	0.9174	0.1980	0.5039	0.9140	1.1524	0.7052	37.52	0.0109	25.44	17.85	0.9845	1.147
	.9381	.2141	.4928	.8979	1.1428	.6987	38.21	.0223	25.11	17.60	.9672	1.121
	.9587	.2299	.4822	.8815	1.1332	.6922	38.93	.0338	24.83	17.46	.9507	1.097
	.9794	.2455	.4720	.8645	1.1235	.6858	39.69	.0454	24.59	17.24	.9352	1.074
	1.0000	.2609	.4622	.8472	1.1138	.6792	40.48	.0570	24.39	17.10	.9203	1.052

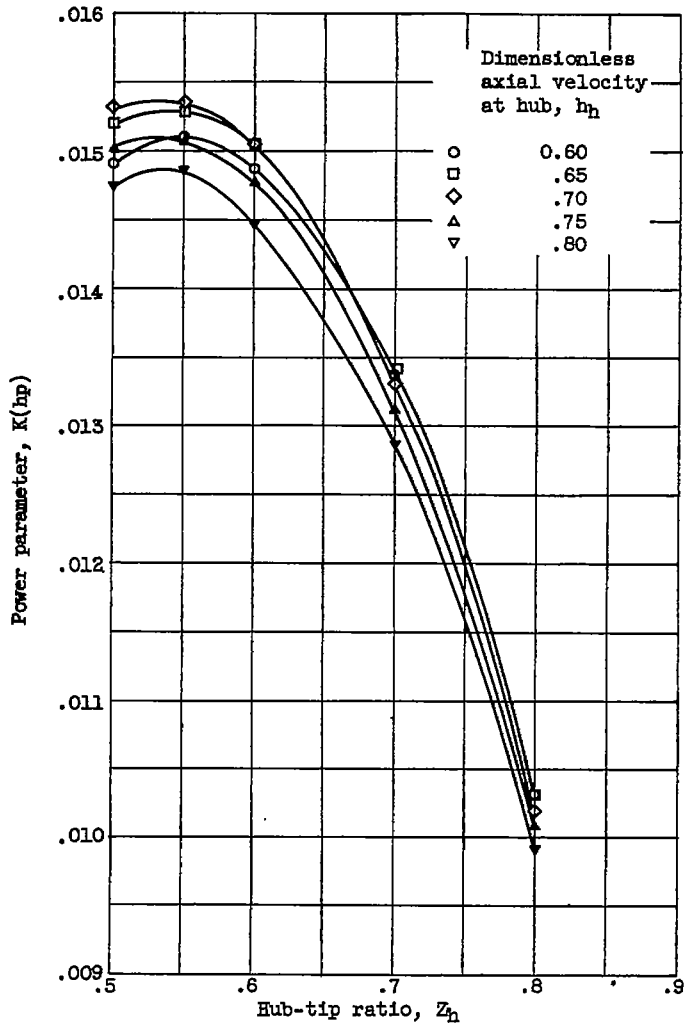

(a) Variation with hub-tip ratio.

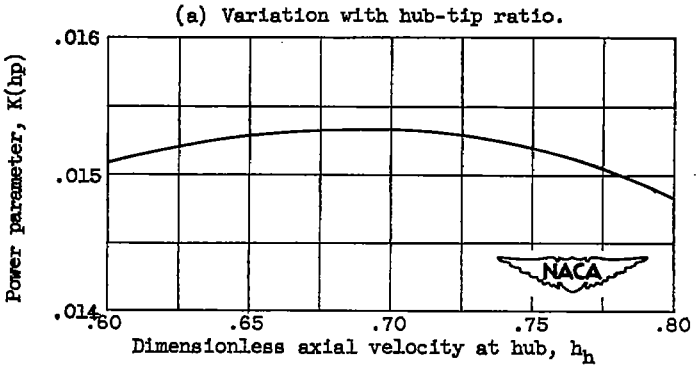

(b) Variation with dimensionless axial velocity at hub for hub-tip ratio of 0.55.

Figure 1. - Variation of power parameter. Loading limit, 0.80; average axial Mach number, 0.70.

2494

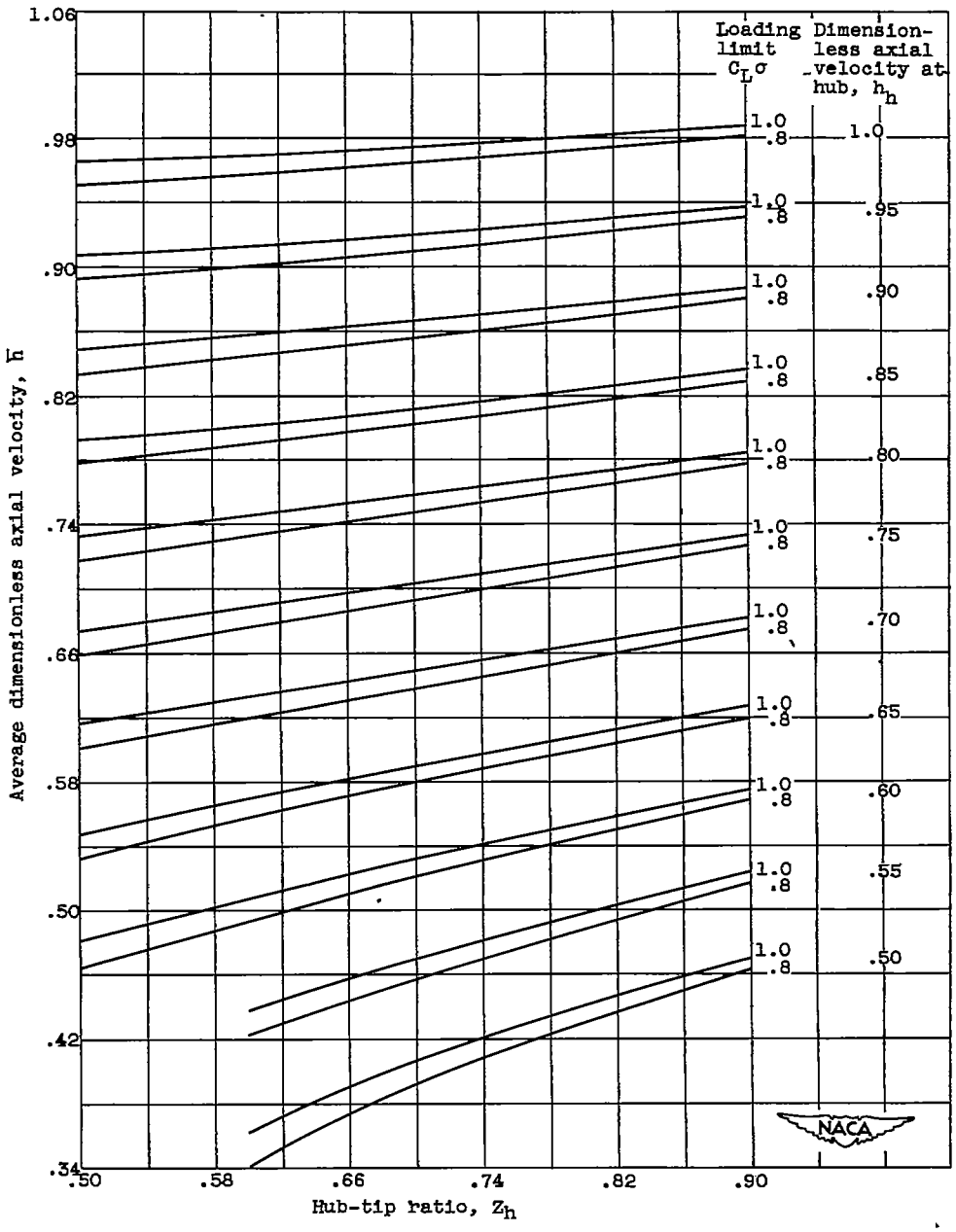

(a) At rotor entrance.

Figure 2. - Chart for determination of average dimensionless axial velocity.

$$\bar{h} = \frac{1}{1 - Z_h^2} \int_{Z_h}^{1} Z \sqrt{4h_h^2 + 2Z_h^2 - 2Z^2 + 4Z_h Y_h \log_e \frac{Z}{Z_h}}\, dZ$$

$$\text{where} \quad Y_h = \frac{C_L\sigma}{2} \sqrt{h_h^2 + \frac{Z_h^2}{4}}$$

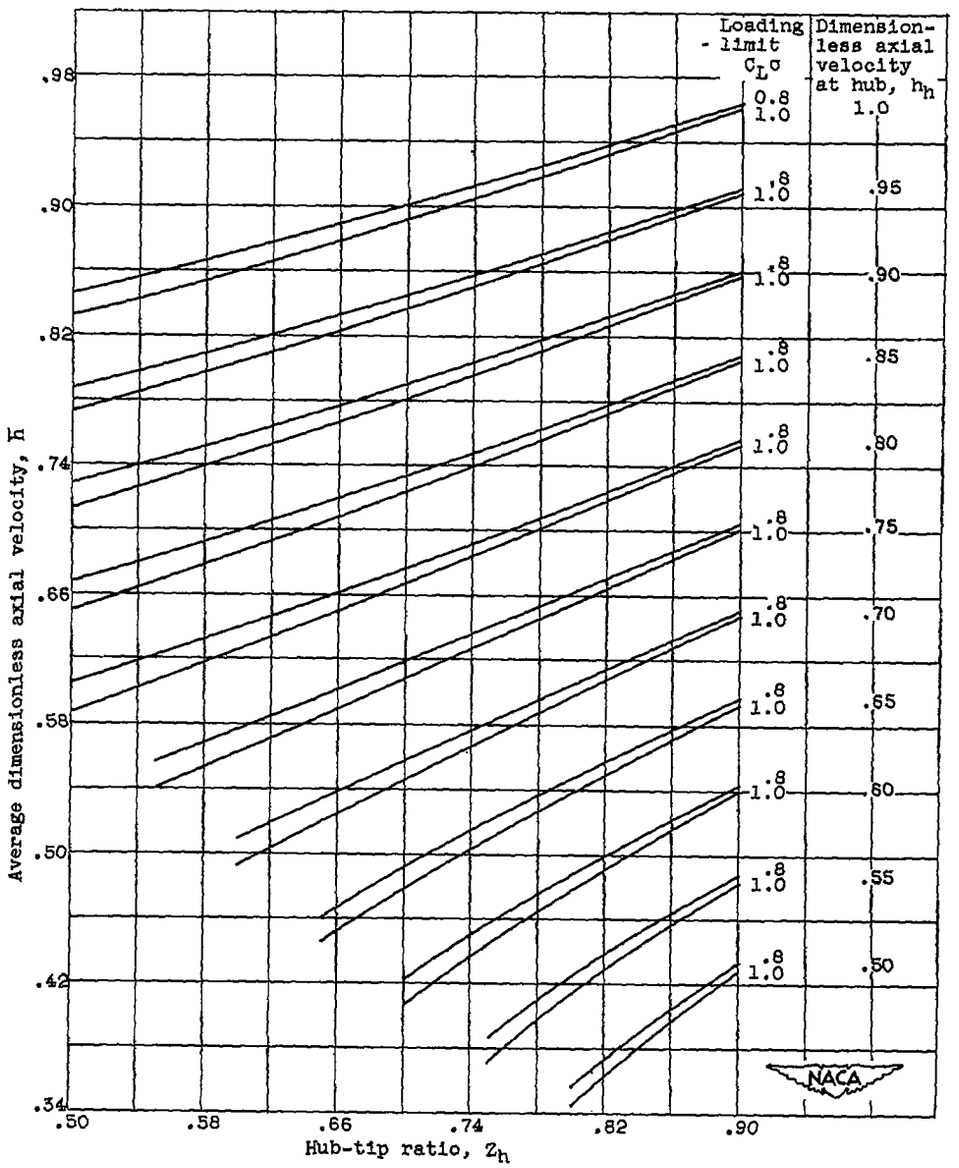

(b) At stator entrance.

Figure 2. - Concluded. Chart for determination of average dimensionless axial velocity.

$$\bar{h} = \frac{1}{1 - Z_h^2}\int_{Z_h}^{1} Z\sqrt{4h_h^2 + 2Z_h^2 - 2Z^2 - 4Z_hY_h \log_e \frac{Z}{Z_h}}\, dZ$$

$$\text{where} \quad Y_h = \frac{C_L\sigma}{2}\sqrt{h_h^2 + \frac{Z_h^2}{4}}$$

2494

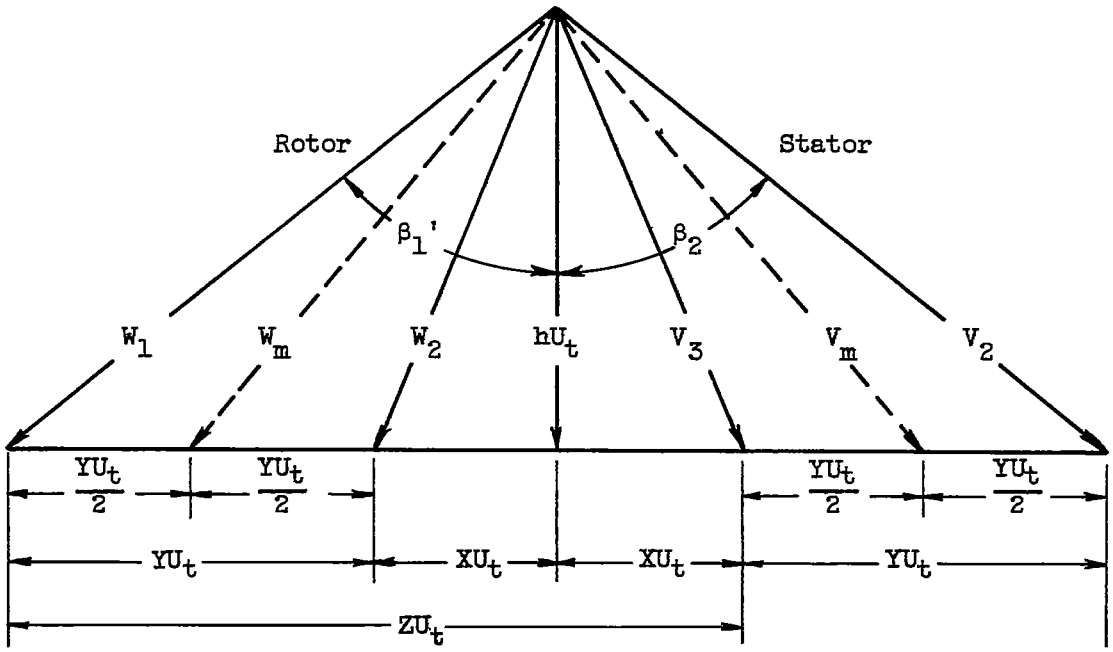

(a) Constant axial-velocity diagram.

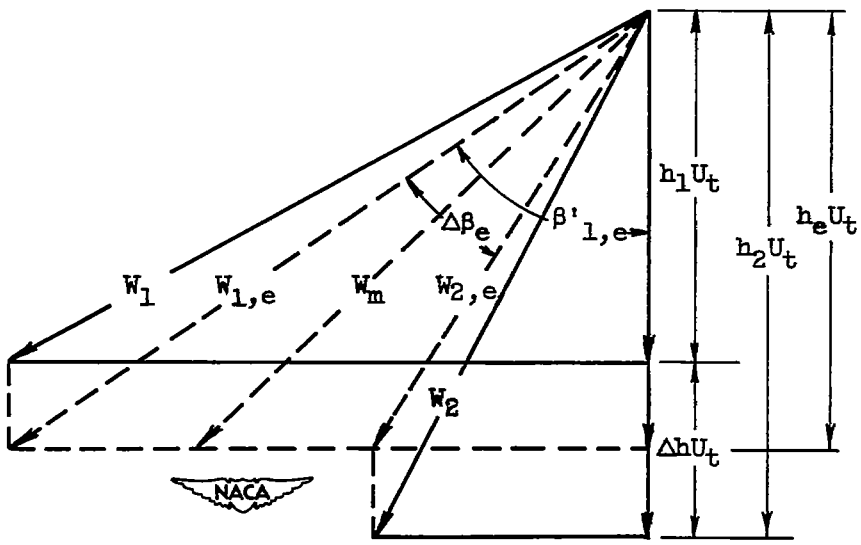

(b) Variable axial-velocity diagram (rotor).

Figure 3. - Velocity diagrams and notation.

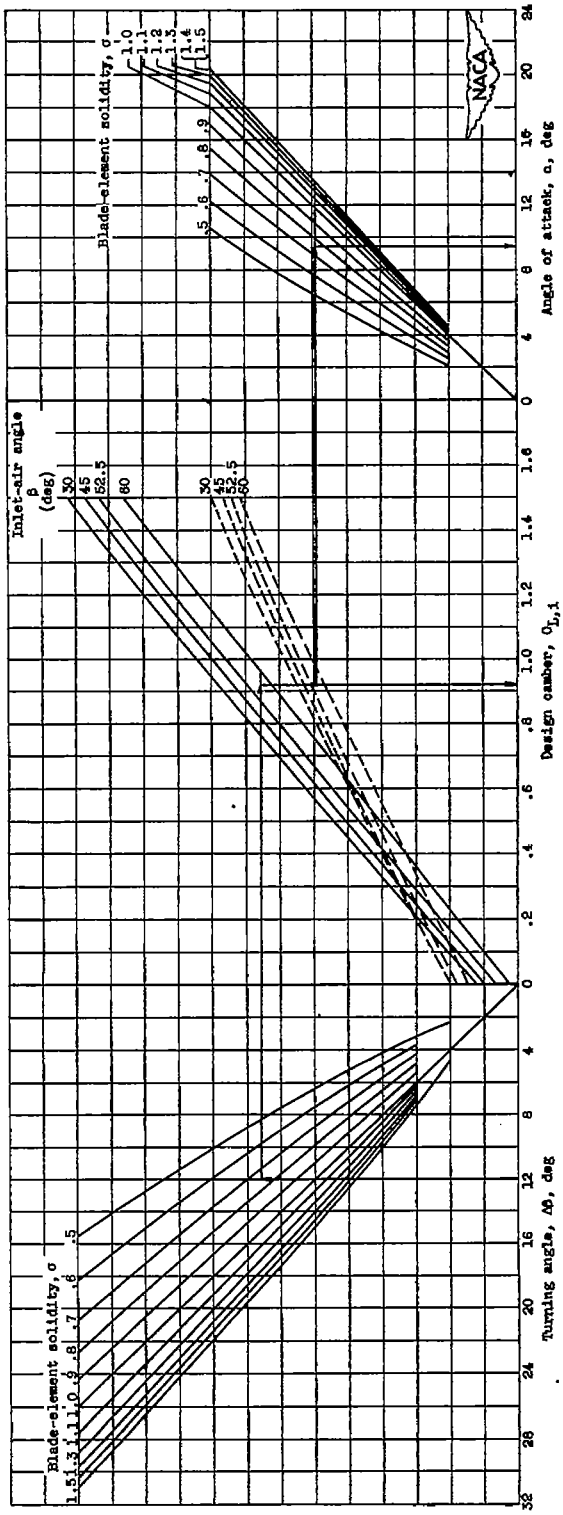

Figure 4. - Design chart for NACA 65-series blower blade sections.

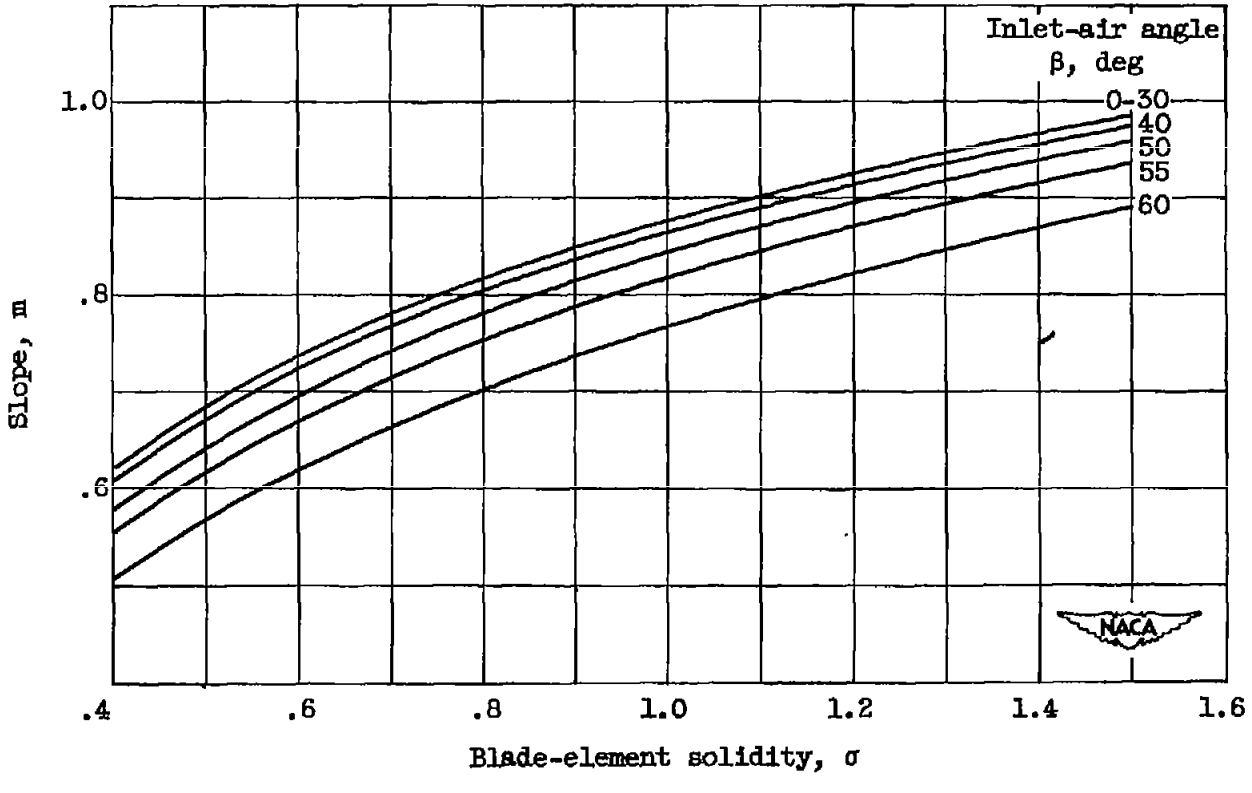

(a) Determination of m in equation $\Delta\beta = m\alpha + b$.

Figure 5. - Design chart for NACA 65-series blower blade sections.

[redacted]

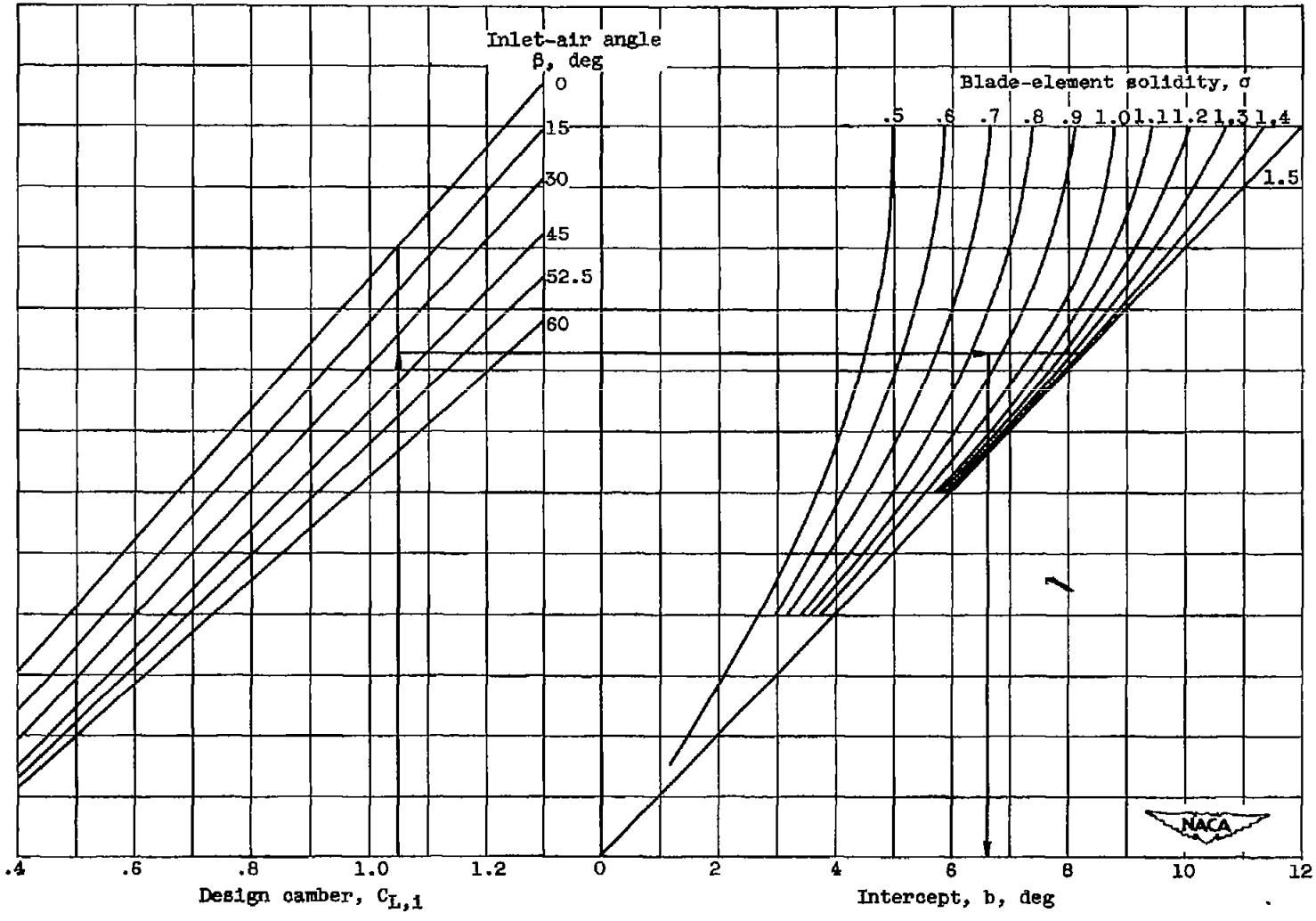

(b) Determination of b in equation $\Delta\beta = m\alpha + b$.

Figure 5. - Concluded. Design chart for NACA 65-series blower blade sections.

[redacted]

2494

2494

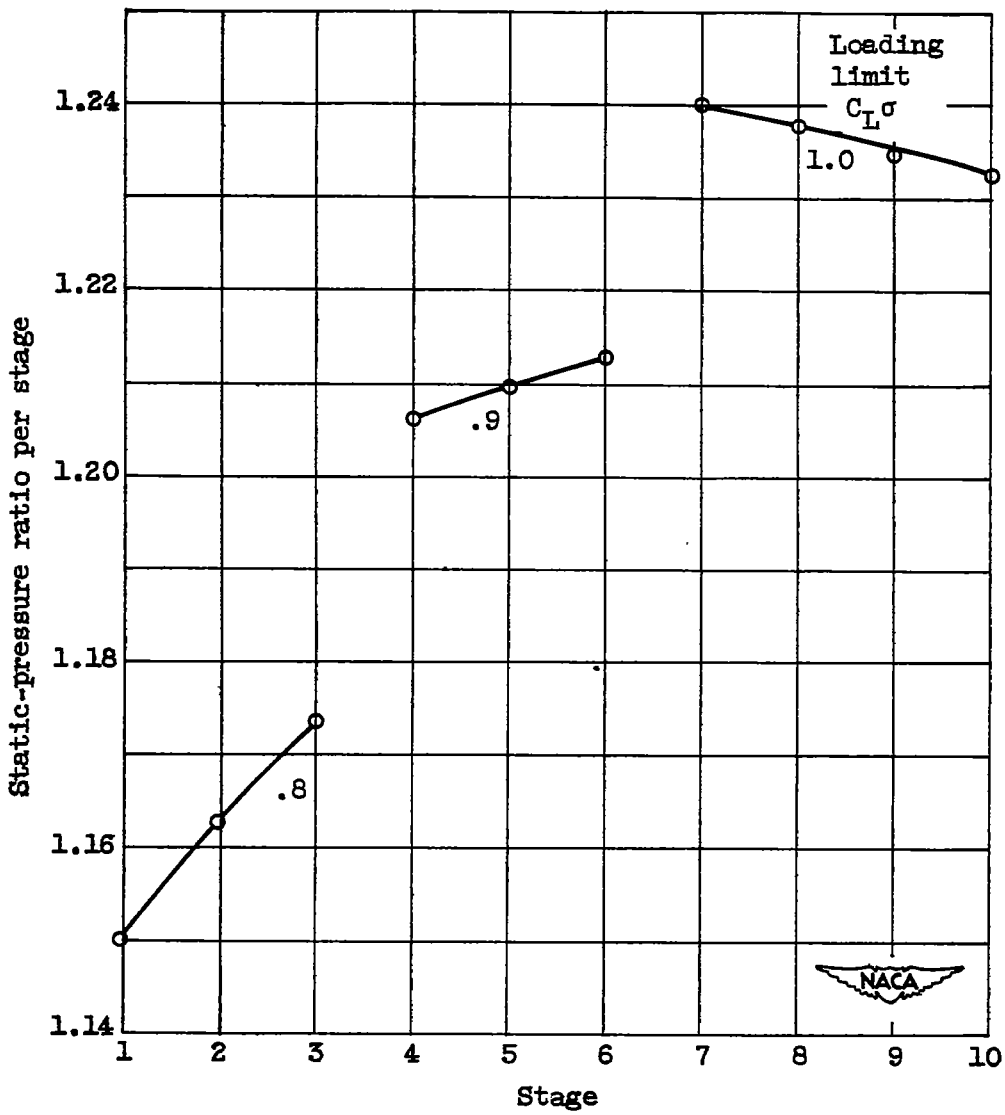

(a) Static pressure of individual stages.

Figure 6. - Pressure-ratio variation through compressor.

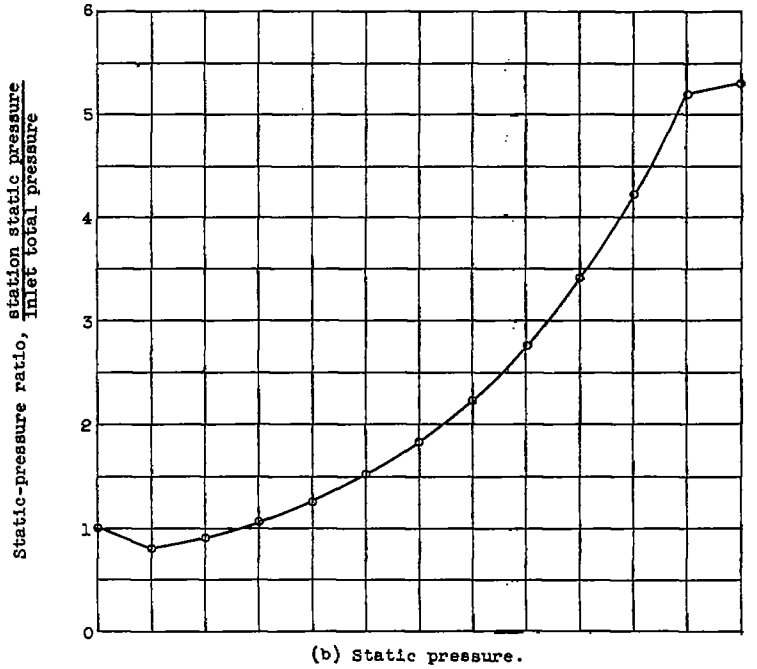

(b) Static pressure.

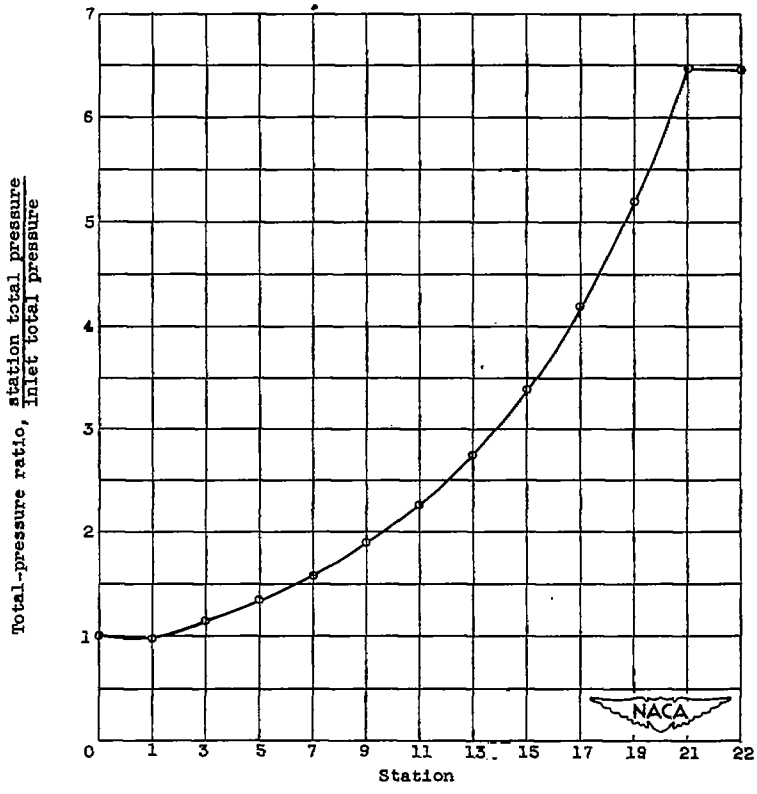

(c) Total pressure.

Figure 6. - Concluded. Pressure-ratio variation through compressor.

2494

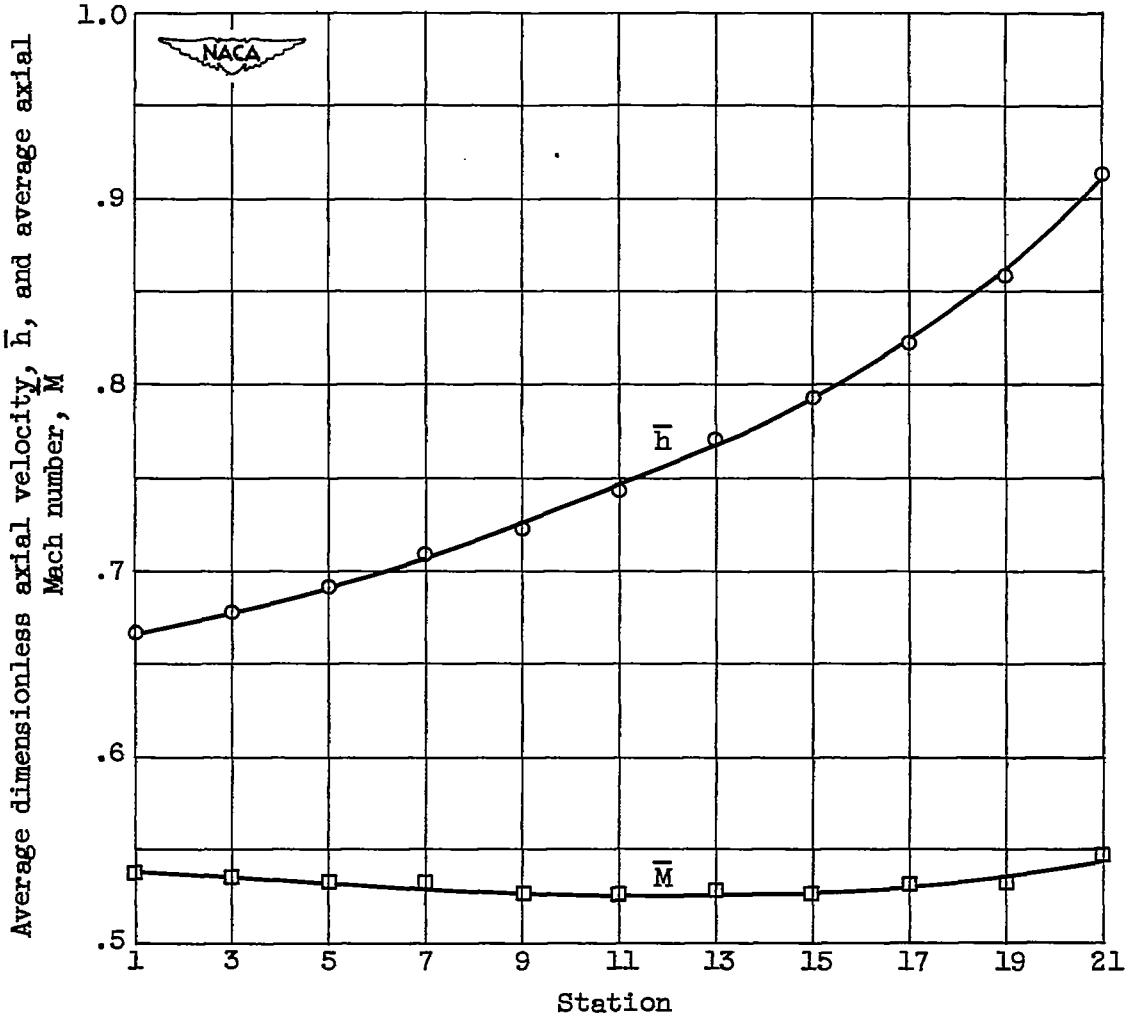

Figure 7. - Variation of average dimensionless axial velocity and average axial Mach number through compressor.

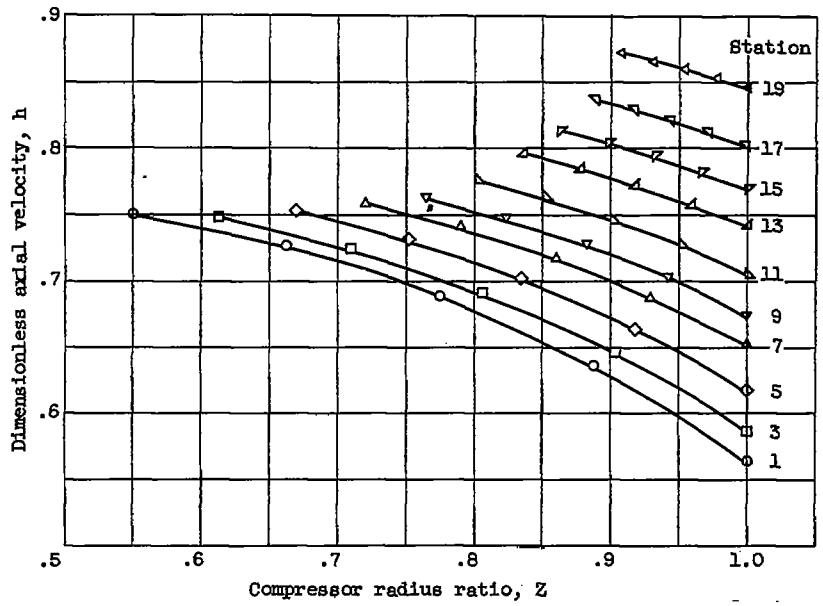

(a) At rotor entrance.

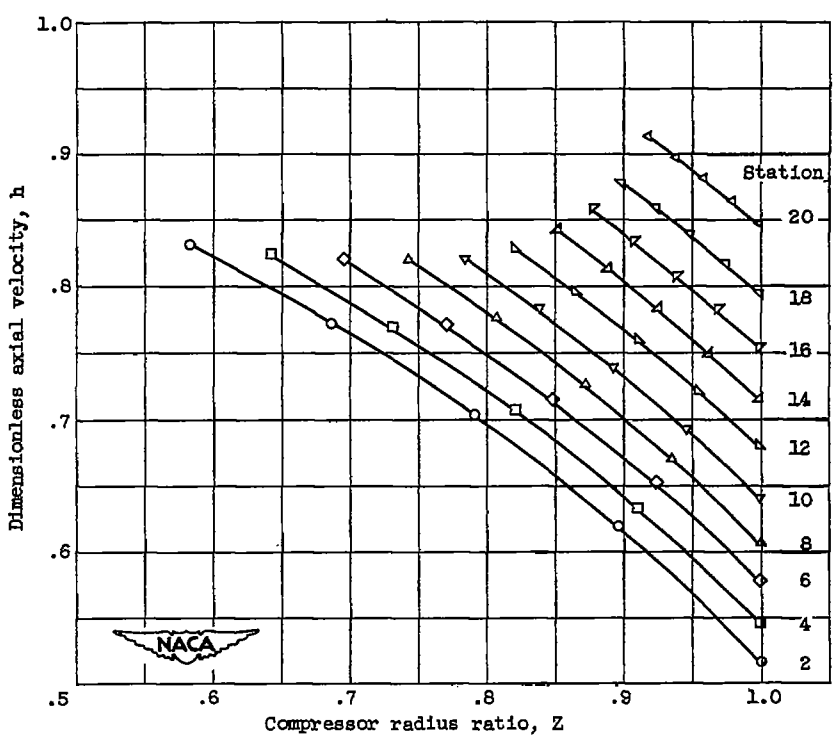

(b) At stator entrance.

Figure 8. - Distribution of dimensionless axial velocity.

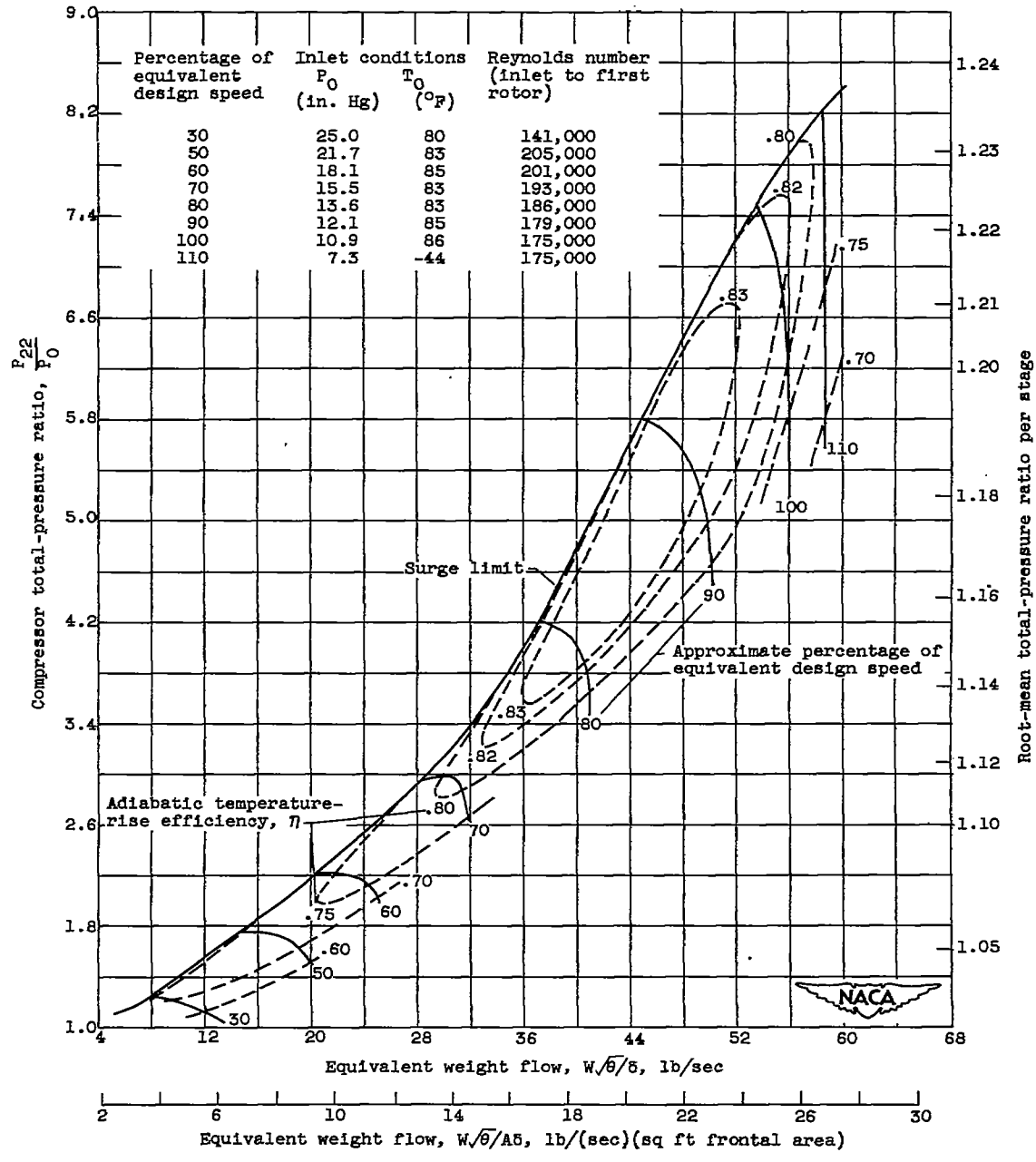

Figure 9. - Over-all performance characteristics of 10-stage axial-flow research compressor.

NACA-Langley - 4-28-52 - 450